



Geophysical and analytical determination of overstressed zones in exploited coal seam: a case study

Dariusz Chlebowski¹ · Zbigniew Burtan¹

Received: 16 September 2020 / Accepted: 28 January 2021 / Published online: 20 February 2021
© The Author(s) 2021

Abstract

A variety of geophysical methods and analytical modeling are applied to determine the rockburst hazard in Polish coal mines. In particularly unfavorable local conditions, seismic profiling, active/passive seismic tomography, as well as analytical state of stress calculating methods are recommended. They are helpful in verifying the reliability of rockburst hazard forecasts. In the article, the combined analysis of the state of stress determined by active seismic tomography and analytical modeling was conducted taking into account the relationship between the location of stress concentration zones and the level of rockburst hazard. A longwall panel in the coal seam 501 at a depth of ca. 700 m in one of the hard coal mines operating in the Upper Silesian Coal Basin was a subject of the analysis. The seismic tomography was applied for the reconstruction of P-wave velocity fields. The analytical modeling was used to calculate the vertical stress states basing on classical solutions offered by rock mechanics. The variability of the P-wave velocity field and location of seismic anomaly in the coal seam in relation to the calculated vertical stress field arising in the mined coal seam served to assess of rockburst hazard. The applied methods partially proved their adequacy in practical applications, providing valuable information on the design and performance of mining operations.

Keywords Underground mining · Hard coal mining · Rockburst hazard · State of stress · P-wave field · Analytical modeling · Seismic tomography

Introduction

In addition to measures taken to effectively cope with rockburst hazard, a broadly understood rockburst prevention strategy involves the assessment of hazard levels in relation to specific geological and mining conditions in the area of the planned mining operations (Zorychta 2003). Geophysical methods, in particular seismological and seismoacoustic observations and seismic measurements in the form of profiling or seismic tomography, play an important role in the assessment of rockburst hazard levels (e.g., Dubiński 1989; Pilecki 1999; Kormendi et al. 1986; Luxbacher et al. 2008; He et al. 2011; Szreder et al. 2008; Dou et al. 2012; Cai et al. 2014; Mutke et al. 2015; Wang et al. 2016; Cao et al.

2016; Czarny et al. 2019; Marcak and Pilecki 2019; Li et al. 2020). Depending on the geological and mining conditions, the selection of the type and scope of adequate preventive measures is based on the results of successively conducted seismic surveys supported by the results of analytical and/or numerical modeling. These methods yield the range and size of stress concentration zones in the rock mass, as well as destressed zones. A vast majority of coal mines in the USCB (Upper Silesian Coal Basin) that are still operational, have to mine very deep lying coal seams in confined conditions. They are caused, inter alia, by the presence of coal seams remnants from previous mining operations or geological disturbances (Zorychta and Burtan 2008). They give also rise to high-energy seismicity and thus increase the risk of rockbursts in underground workings. The presence of constraining factors leads to changes in the state of stress and, consequently, in the changes of density of elastic energy in rock formations (Zorychta 2003; Chlebowski 2013).

The aim of this study is a combined analysis of changes in stress distributions and the resulting rockburst hazard level assessments based on seismic tomography (A-G 2009–2010)

Communicated by Michal Malinowski (CO-EDITOR-IN-CHIEF)/Zenon Pilecki (Guest Editor).

✉ Dariusz Chlebowski
chlebo@agh.edu.pl

¹ AGH University of Science and Technology, Kraków, Poland

and analytical modeling (BN-T 2008). Research work was conducted in one of the coal mines operated by Polska Grupa Górnicza S.A. and results were obtained from the mining longwall 09a in 501 coal seam. Seismic tomography was applied to reconstruct the P-wave velocity field in the coal seam, yielding the stress redistribution zones (Nolet 1987; Dubiński 1989; Goszcz et al. 1989; Lo and Inderwiesen 1994; Kormendi et al. 1986; He et al. 2011; Li et al. 2020).

Analytical modeling relies mostly on rock mechanics classical solutions having relevance to stress and deformation relations arising in mined-out coal seams (Sałustowicz 1968; Pietuchow and Linkov 1979; Kłeczek et al. 1987; Zorychta 2003; Gil 1991; Karfakis and Wu 1995; Zhao et al. 2000; Bańka 2004; Wang et al. 2006; Yang et al. 2018). In this study a geomechanical model of the longwall mining system was developed, underpinned by the theory of bending plates rested on a deformable supports (Gil 1991; Zorychta 2003). The governing differential equations of the deflection line were solved and distributions of vertical displacements and stress state in the research region were established.

Geological and mining conditions in the test area

The longwall panel 09a with a coal seam height of 3.6–4.2 m, length of 130 m and panel length of 690 m, located within the enclosed portion B of the coal seam 501 at a depth of 700 m was selected as the case study. The longwall 09a was rated to be the third-degree rock burst hazard category according to the formal regulations, the third self-heating propensity category, the fourth methane hazard category, class B dust hazard and the first and second degree of water hazard. Coal seam was mined by the shearer system with a roof caving (Fig. 1). The longwall operation started with a cut-through in the goaf zone of the previously

exploited panel no. 09 and continued along the goafs of another longwall 08 eastbound, between main headings IXa (bottom heading, from the south) and Xb westbound (top heading, from the north).

In the research area, the thickness of coal seam 501 is in the range of 3.6 to 5.4 m, with a dip at a variable angle of about 4°–6° in the south-western direction. There is a layer of sandstone with a thickness of 3.1–7.8 m directly in the roof, then a layer of clay slate locally with carbon inserts with a thickness of 0.3 to 0.5 m, and further a layer of sandstone with a thickness of 11.8–14.2 m. Within the floor of the 501 coal seam, there is a clay slate with a thickness of 0.6 to 0.9 m, which is an intercalation between coal seam 501 and 510, and then coal seam 510 with a thickness of 9.8–11.6 m. There are faults found by mining works, including longwall # 09a with throws of 0.5 and 1.8 m, respectively, and the Xb west heading with a throw of 0.3 m. Moreover, in the area of the panel, there are exploitation edges of the 405, 404/5 and 401 coal seams at vertical distances of about 180, 205 and 270 m, respectively, as well as headings in the 416/418 coal seam at a vertical distance of 50–55 m. Average values of strength parameters determined on the basis of penetrometric tests for coal seam are 12.0–31.2 MPa, sandstone—19.5–72.0 MPa, clay—12.0–33.6 MPa and locally occurring slate—16.8–60.0 MPa (Materials 2010).

Seismic tomography methodology and analysis of results

Seismic tomography was aimed to assess the rockburst/seismic hazard, resulting from critical stresses arising in the coal seam or on the immediate roof/floor rock layers and in the area alongside the panel length 09a/501.

The concentration stress zones give rise to positive seismic velocity anomalies A_s , which is expressed by the formula (Dubiński 1989):

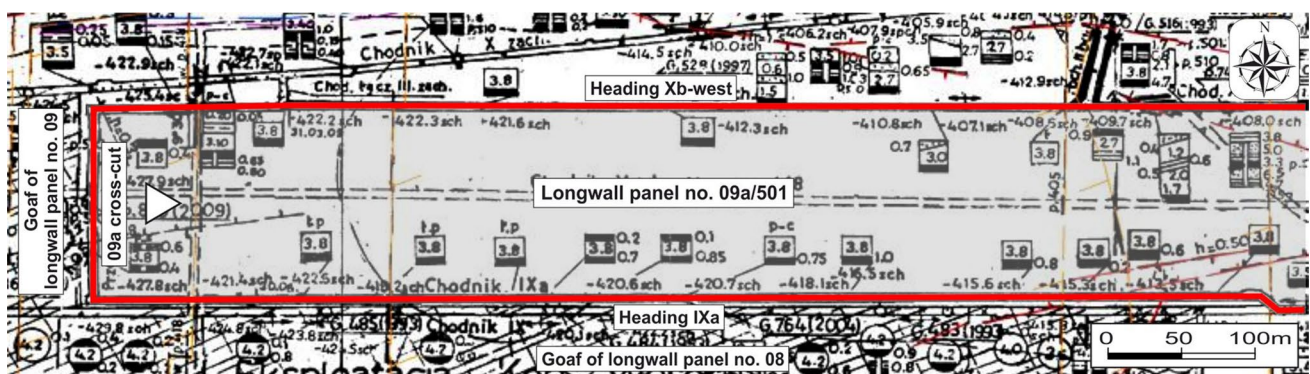


Fig. 1 Fragment of coal seam map with longwall 09a/501 (Materials 2010)

Table 1 Rockburst hazard increase ratings based on seismic anomaly (Dubiniński 1989)

Stress increase rate	Stress increase	A_s [%]	Stress increase [%]
0	None	< 5%	< 20
1	Low	5 to 15	20 to 60
2	Medium	15 to 25	60 to 140
3	High	> 25	> 140

Table 2 Destressing effectiveness based on seismic anomaly (Dubiniński 1989)

Destressing rating	Destressing effectiveness	A_s [%]	Stress decrease [%]
0	None	0 to − 7.5	< 25
1	LOW	− 7.5 to − 15	25 to 55
2	Medium	− 15 to − 25	55 to 80
3	High	< − 25	> 80

$$A_s = \frac{v_p - v_p^0}{v_p^0} \times 100\% \quad (1)$$

where v_p —measured P-wave velocity, v_p^0 —reference velocity.

The value of the reference velocity, associated with the depth (H) of the control point, can be obtained from measurements or derived from the formula (Dubiniński 1989):

$$v_p^0 = 1200 + 4,83(\pm 0,077)H^{0,76(\pm 0,028)} \quad (2)$$

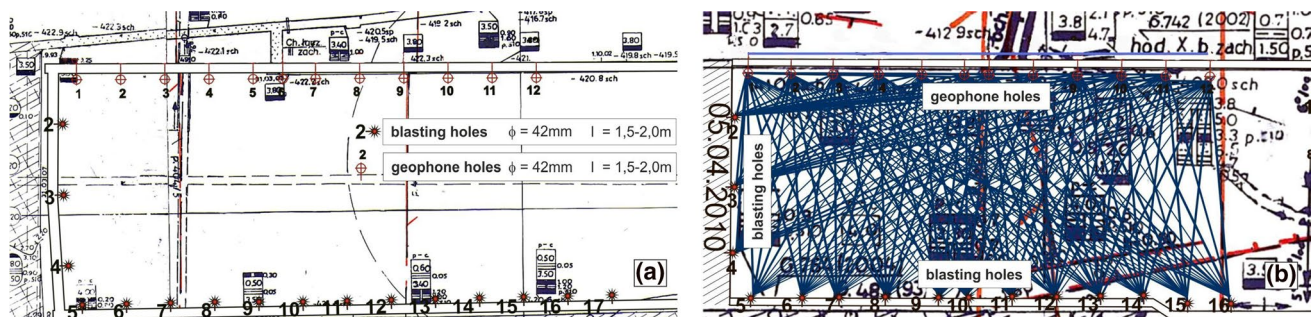
Three categories of seismic hazard ratings are proposed. Alongside three respective rockburst hazard categories, from small through medium to large, are defined by the value of seismic anomaly (A_s). The ratings of rockburst hazard increase in USCB mines, based on seismic anomaly value, are given in Table 1.

For mining operations that involve destressing, seismic anomaly value will yield the effectiveness of destressing. For this purpose Table 2 is proposed to evaluate the scale of expected stress decrease.

Seismic tomography was performed in four consecutive measurement series. As part of the 1st, 2nd and 3rd series, the test was carried out between the Xb west heading, front of the longwall and IXa heading, and additionally for the 4th series in dip-road III (Fig. 1). The seismic tomography involved the longwall face zone over the length about 350 m from the cut-out (series 1), the Section 300 m from the front of the local heading in the next two series (2nd and 3rd) and the section of 290 m of the length in case of the last series (4th). A wavefield was induced by small explosive charges detonated in blast holes located in the IXa heading, spaced 25 m, and in the cut-through, spaced 40 m, and additionally in the 4th series, in the dip-road III, within 40 m distance from Xb west heading. Thus generated seismic waves were recorded using 28 Hz geophones in the south sidewall of Xb west heading (distance between the geophones 15–20 m). The recording time was about 500 ms and sampling frequency 1 kHz.

The aim of the measurements was to obtain technically correct seismograms that would determine the onset of the P-wave propagated in the coal seam. The configuration of geophones and excitation points was determined by the layout of existing and accessible headings (Fig. 2).

In the next step, P-wave velocities were calculated and the adequacy of the calculation procedure was verified by statistical analysis of sets of ray lengths, travel times and ray velocities. Correlation analysis and linear regression of the paths and arrival times allow the systematic errors involved in individual path measurements to be eliminated through introduction of the constant correction, which is of key importance when registering the first arrival times of refracting waves. The analysis of correlation and linear regression in the ray path-velocity system proves useful in examination of seismic records in the context of refracted wave propagation in the fractured medium. In the next step, the velocity wavefields were reconstructed by the

**Fig. 2** Layouts for seismic tomography: **a**—series I, **b**—series III

linear tomography utilizing the iterative SIRT (Simultaneous Iterative Reconstruction Technique) (Krajewski et al. 1989; Ruban et al. 1993; Hosseini et al. 2012). The entire longwall plane was decomposed into cells with the dimensions 20×20 m. Iterations procedure was repeated until the error involved in reconstruction was effectively reduced to the noise level. Accordingly, the measure of the reconstruction error was the standard deviation of the set of differences between the measured and computed times, derived basing on the reconstructed velocity wavefield along the seismic ray paths.

To the extent required for the purposes of combined analyses with analytical models, the results of seismic surveys were limited to the presentation of selected velocity field parameters only in the coal seam and illustrated in the form of contour maps showing the variability of:

- P-wave velocity (Fig. 3),
- Seismic velocity anomaly (Fig. 4),

In two selected measurement series—series I and III given as examples, though the cognitive aspects are the most interesting.

The results of seismic tomography show that P-wave velocity in the coal seam in the research region changes significantly in the range of 1,650–2,200 m/s for both measurement series, with an average of 1,980 m/sec. The variability range of ray velocity appears to be smaller, slightly exceeding 5%. In case of the I series, local high velocity zones (more than 2,125 m/s, anomaly more than +9%) occur along the Xb west heading up to 30 m from the longwall and in the vicinity of the cut-through up to 20 m from this heading. Similarly, for series III, increased velocity zones, more than 2,125 m/s, anomaly +9% are found at the Xb west heading up to 30 m from the front of the longwall average. Moreover, in both series, local zones of increased P-wave velocity were observed along the panel length of the designed longwall section, excluding the headings (Fig. 3).

Assuming that the seismic anomaly distribution is related to redistribution of stresses in the coal seam, a positive seismic anomaly in excess of +15% indicates a significant stress increase in relation to the value regarded as average (Table. 1). A negative seismic anomaly below −7.5% (Table. 2)

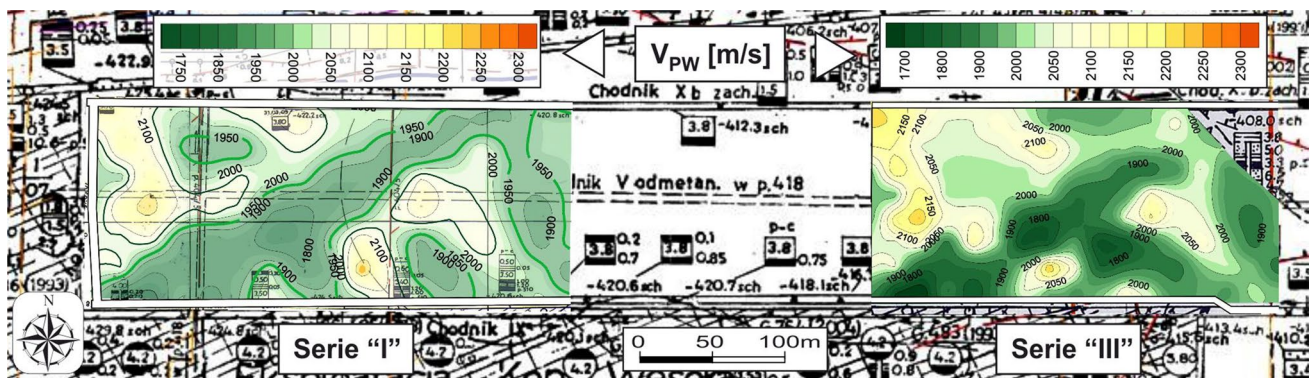


Fig. 3 P-wave velocity distribution in coal seam 501 in longwall 09a/501

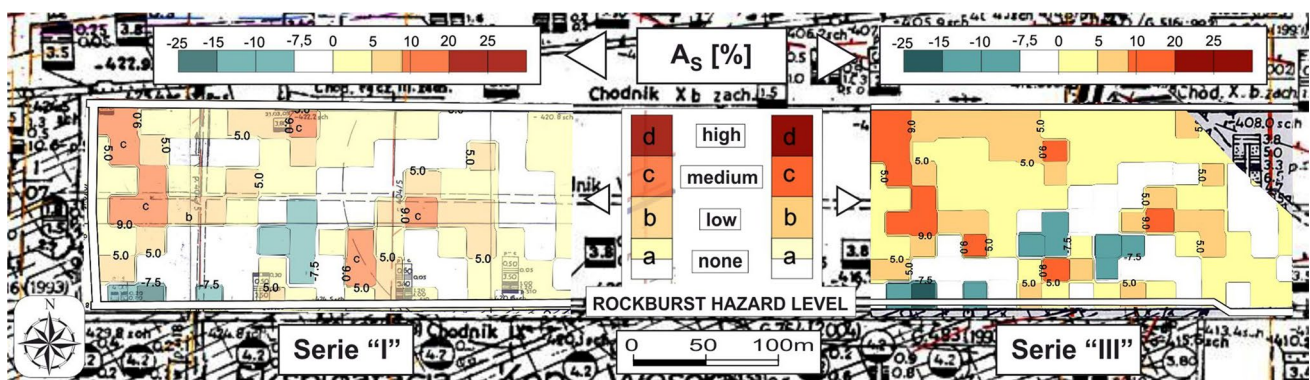


Fig. 4 Distribution of seismic anomaly in coal seam 501 in longwall 09a

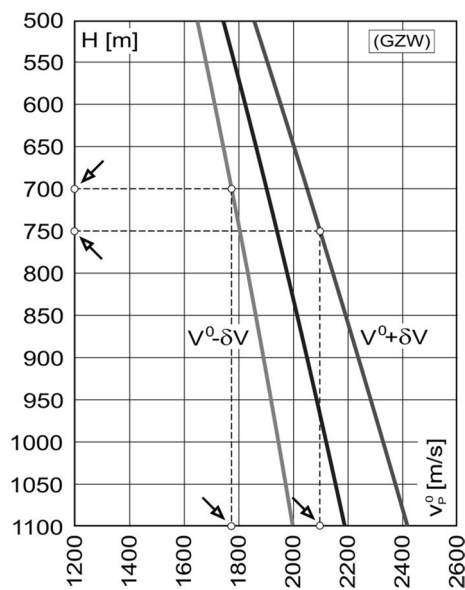


Fig. 5 Reference velocity of longitudinal wave in the coal seam 501 (depth 700–750 m) (based on Dubiński 1989)

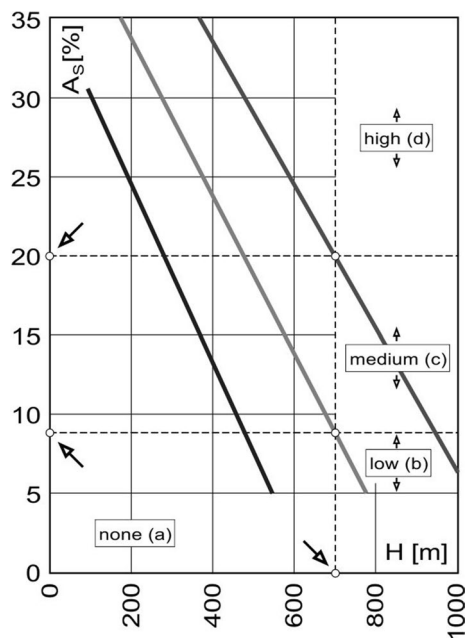


Fig. 6 Rockburst hazard level in the function of seismic anomaly (based on Dubiński 1989)

indicates the weakening zones of the coal seam, where the structural disruption processes are very likely. Based on the relationship between reference velocity and depth and rockburst hazard variability (Dubiński 1989) (Figs. 5, 6), it can be concluded that an increase in positive seismic anomaly of more than +20% resulting from an average stress increase will lead to elevated rockburst hazard level d in Figs. 4, 6. In

the studied area, no hazard level a in Fig. 4 and low hazard b in Fig. 4 dominate, with no high hazard level d. Medium-level rockburst hazard is reported in local areas, which account for 9–10% of the total area (Fig. 4). The results of series I indicate that the medium level hazard zone includes the Xb west heading at a distance of 30 m from the cut-through and the longwall cut-through at a distance of 20 m from this heading. The seismic anomaly may be attributable to the stress redistribution in the vicinity of the interrupted mining operations on longwall 09 and the remaining coal seam south of the tectonic disturbance (20 m). It appears that the coal seam 501 was not destressed during the previous mining operations in coal seams 405 and 404/5, and there are local stress increases and decreases in the area alongside the edges of these coal seams. The location of the indicated areas does not also confirm a direct causal relationship with the edge of coal seam 405. With regard to the results of the third series, it can be said that the dominant factor causing stress redistribution was the progress of a longwall face. The zone with medium level rockburst hazard includes the surroundings of the Xb west heading on the section of 30 m from the front and the front of longwall 09a on the section of 35 m from the Xb west heading. Locally, the medium level rockburst hazard zone extends up to 50 m in front of the longwall, while the remaining hazard zones are fragmented alongside the panel length and do not include headings (Fig. 4). Enhanced seismicity in the discussed zones can be expected when the longwall front advances toward them at a distance of about 50 m.

Taking into account the above-mentioned considerations, seismic anomalies indicate the possibility of stress concentration in the studied area. In the longwall panel 09a/501, different energy of tremors can be expected in panel sections indicating low and medium rockburst hazard levels associated with structural disruption of the coal seam and of its immediate surroundings rock layers.

Analytical modeling methodology and analysis of results

The main factors determining the rockburst hazard in the studied area are: stress state in the mining area, physical and mechanical properties of the rock mass and induced seismicity, especially occurrence of high-energy seismic events. A necessary condition triggering the rockburst in an underground excavations is the critical stress loads in hazardous areas (Zorychta 2003; Chlebowski 2013). The stress arising in the rock mass as a consequence of deformation processes can be expressed by a stress indicator, and recalling the Mohr–Coulomb criterion it is defined as a function of strength parameters and principal stresses (Sałustowicz 1968; Kłeczek 1994). The magnitudes of the state of stress

components in the investigated coal seam are determined, in turn, by its depth, the impacts of coal seam remnants and tectonic disturbances. Moreover, they also depend on the employed mining method technology, as well as type and geometry of excavations (Kłeczek and Zorychta 1990; Zorychta and Chlebowski 1998; Zorychta et al. 1999; Chlebowski 2009). In the context of modeling deformations and stress conditions in the rock mass, analytical or numerical methods have gained in importance in the long-term design of mining operations. They can be used to estimate the rockburst hazard during mining operations.

The rockburst hazard assessment for the longwall panel no. 09a/501 is based on the results of the analytical modeling and thus derived countour maps, yielding the variability of:

- The vertical stress (σ_z), as a superposition of gravity-induced stresses and the presence of remnants of previous mining operations and geological disturbances (Fig. 7),
- Stress concentration factor (k), expressed as the quotient of vertical stresses and lithostatic stresses (p_z) (Fig. 8).

The developed model of the rock strata takes into account the nonlinear characteristics of the coal seam deformability and linear deformability of the roof/floor rock layers. The influence of constrained conditions is modeled by an uneven distribution of external static loads (Chlebowski 2013). Simulations were supported by a computer program developed by the Authors and the calculation procedure relied on differential equations of equivalent roof bending in consideration of a variety of aspects involved in mining operations (the presence of goafs, unmined coal body and available working space). The fact that the original structure of the coal body could thus get fractured was taken into account. The system of heterogeneous linear equations was solved assuming the boundary conditions determining the continuity of roof bending, inclination and internal forces acting at characteristic points in the model. Thus derived formulas yielding the distributions of displacements and vertical stress within the coalbed were implemented into the program, partly in the form of numerical procedures. The cartesian coordinate system (emulating the geometry of the mined lot) was used in calculations, with the step ensuring the sufficient accuracy of results (the basic grid 5×5 m). Prior to the calculation procedure all relevant data

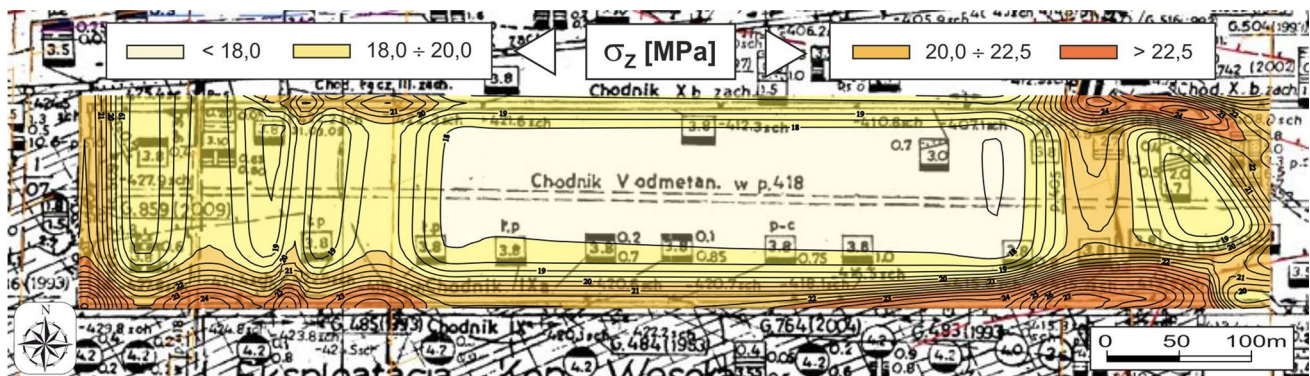


Fig. 7 Map of vertical stresses in coal seam 501 in longwall panel 09a/501

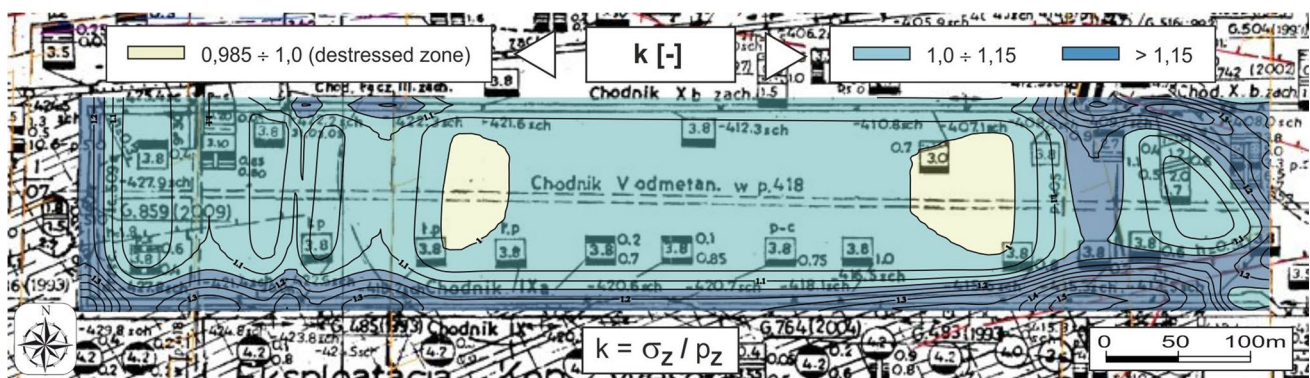


Fig. 8 Map of stress concentration factor k in coal seam 501 in longwall panel 09a/501

were loaded, including mechanical parameters of the rock strata and information about the current mining conditions in the area (such as the presence of mining remnants).

Contour maps (Figs. 7, 8) illustrate the mining conditions in the analyzed area after the completion of longwall mining operations in the panel 08 in the southern section and 09 in the western section, but prior to mining of the longwall panel 09a (Fig. 1). This means, the impact of longwall face progress are neglected, permitting us only to estimate the potential rockburst hazard during the mining of coal seam 501.

The calculations indicate that the state of stress within the analyzed longwall panel, between IXa and Xb west headings, in the cut-through and in the panel end sections tends to vary. These stress variations can be attributed to the interactions of extensive goafs, the presence of remnants of previous mining operations in the surrounding rock strata as well as by sedimentation and fault disorders. The analysis of modeling results reveals that the vertical stress values are in the range from 17.4 to 27.6 MPa (Fig. 7). These are found to be fragmentarily higher than the uniaxial compressive strength of coal seam 501. Consequently, local critical intensity zones will appear in the form of fracture zones. It means that during the mining operations on longwall 09a, with additional impacts produced by the longwall face, rather the low-energy tremor hazard may be enhanced reaching 10^3 J and 10^4 J.

These observations are fully confirmed by the distribution of the stress concentration factor k . The variability range of k is 0.985 to 1.55 in the longwall panel area (Fig. 8). Its value below 1.0 indicates the presence of destressed zones in the coal seam. The stress concentration zones revealed in the distribution diagrams (darker blue color) are attributable to the superposition of interactions from the goafs of longwall 08 on the southern side and 09 on the western side, the presence of faults with throws of up to 1.6 m and the edge complex in coal seams 405, 404/5, 401 as well as to the disappearance of coal seam 501 in the north-eastern corner of the panel. Relatively, the most favorable state of stress, similar to the lithostatic stress of the order of 18 MPa, factor $k \sim 1$, is registered in the middle section of the panel in an area practically free of confined mining and geological conditions.

Analytical modeling results can be interpreted with reference to seismicity prognosis undertaken as a part of development works. Since the presence of heading impacts on changes in stress and elastic energy in the surrounding strata in a lesser degree only, low-energy up to 10^4 J may be registered during the road heading operations. Furthermore, the advance of the longwall face 09a must impact on compact sandstone layers. These formations may become periodically activated with a potential to trigger high-energy tremors. Energies of most events with foci in the burst-prone strata overlying coal seam 501, should not exceed $7 \cdot 10^5$ J. The

greatest probability of a rockburst occurrence is associated with the designated stress concentration zones. Since the rockburst hazard is a resultant of the state of stress in the coal seam and the predicted seismicity of the rock strata, it should be assumed that the longwall advance should give rise to medium- and locally high-level hazard. Longwall headings, especially the IXa heading, will be exposed to the highest-level hazard.

Effectiveness of the methods

Analytical modeling and the first series of seismic tomography were taken before commencement of mining operations on longwall 09a. Seismic surveys in subsequent test were conducted when mining operations on longwall 09a were in progress. Therefore, full information on induced seismicity and rockburst hazard levels are available in order to estimate the validity of rockburst hazard assessments, and to formulate reliable conclusions through results obtained by analytical and seismic methods. According to information received, a total of 2,566 seismic events were registered during the longwall construction period, including 7 with the energy of the order of 10^5 J (maximum tremor energy $5.5 \cdot 10^5$ J), 102 of the order of 10^4 J (Fig. 11), 1,019 of 10^3 J (Fig. 10), 1,438 of the order 10^2 J (Fig. 9) (Materials 2010). The total energy generated by these tremors amounted to $8.7 \cdot 10^6$ J, equivalent to the value of the unit energy intensity of about 17 J/t. Taking into account analogous data characterizing the seismic activity of the remaining longwalls operated in the area (the analyzed panel was selected as the last one in the series of longwall operations), it appears that the relative rockburst hazard accompanying the advance of longwall 09a was average. In addition, dynamic events such as rockbursts did not occur, despite seven such events being recorded during previous longwall operations.

The theoretical maximum tremor energy was not exceeded, and the adequacy of the applied calculation procedure was thus verified. To account for specificity of the stress state assessments, a more profound statistical analysis of recorded low-energy seismic activity seems justified. Such seismic activity is typically revealed through the effects of disruption of the primary structure of the rock mass. In the general population of recorded seismic events, both spontaneous and invoked by prevention, 99.7% tremors were found to be in the low-energy range below $1 \cdot 10^5$ J, of which 10^4 J was about 4% (Fig. 11), of 10^3 J about 40% (Fig. 10), and of 10^2 J about 56% (Fig. 9). None of the tremors, including high-energy ones, posed a direct threat to the staff safety, which must be the consequence of highly effective preventive measures.

With reference to the distribution of epicenters of low-energy tremors (Figs. 9, 10, 11), it can be stated that

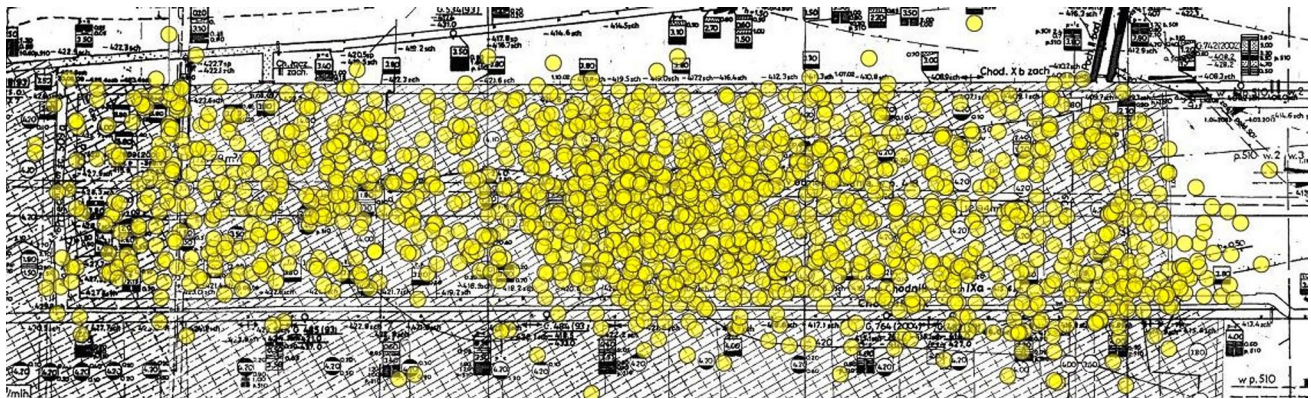


Fig. 9 Location of tremor foci with energy of 10^2 J in longwall 09a/501 (Materials 2010)

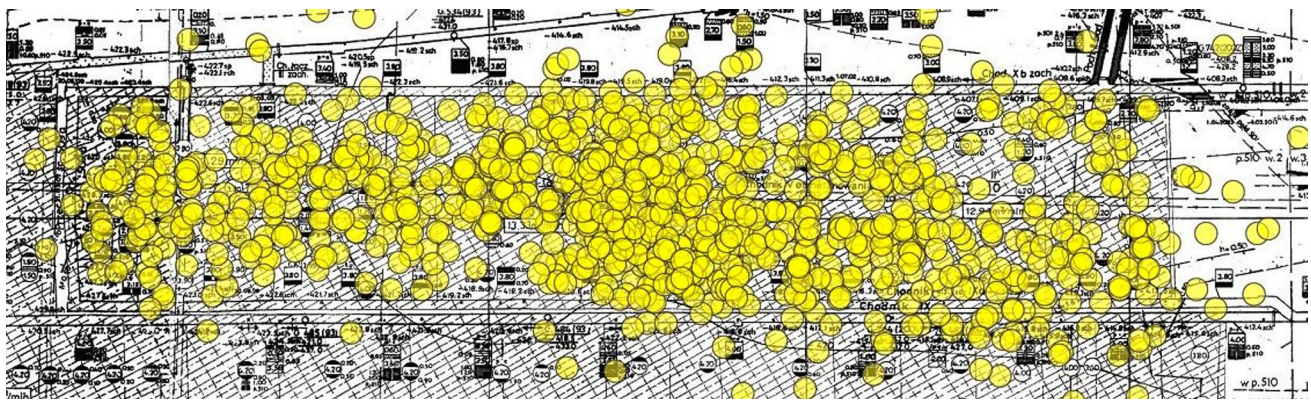


Fig. 10 Location of tremor foci with energy of 10^3 J in longwall 09a/501 (Materials 2010)

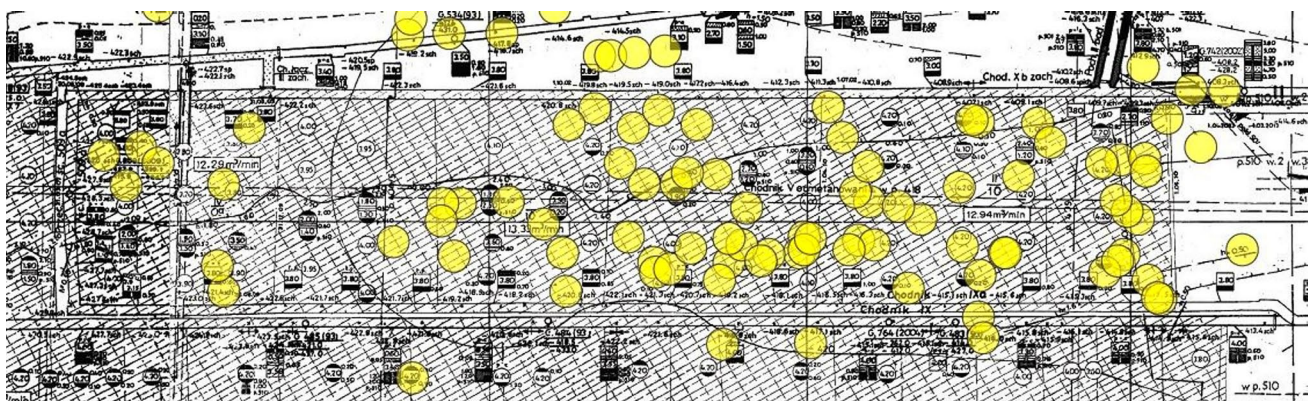


Fig. 11 Location of tremor foci with energy of 10^4 J in longwall 09a/501 (Materials 2010)

regardless of the energy class (10^2 J, 10^3 J, 10^4 J), the distribution of seismic events is rather random, poorly correlated with the seismic anomalies (Fig. 4) and stress concentration areas in the coal seam (Figs. 7, 8). A small number of tremors were registered outside the area considered in this

study. It encompasses nearly the entire northern part of the longwall panel 09a and the goafs of the adjacent southern longwall panel. That renders a full and reliable interpretation of modeling results a daunting task, particularly in relation to higher energy seismic events. Consequently, it can be

assumed that such distribution of tremors can be attributed to the presence of a fault zone with a throw of 17–25 m running along the northern border of the deposit area.

Conclusions

The main objective of the analysis was to combine the results of seismic surveys with analytical modeling of stress state to examine the rockburst hazard caused by the processes of destruction in the coal seam and/or its immediate rock layers. The experiment was conducted in the longwall panel 09a in section B of coal seam 501, designated for mining operations. The combined analysis leads us to the following general conclusions:

- The results obtained by the employed seismic tomography and analytical modeling clearly indicate that the state of stress in the coal seam is subject to changes, mostly due to the impact of previous mining operations, both in adjacent as well as distant coal seams, and geological disturbances, especially tectonic origin.
- Analytical modeling reveals the presence of local stress concentration zones in the longwall panel as a consequence of the superposition of the impacts produced by goafs, the edges of mined-out panels and coal seam washout zone.
- The results of analytical modeling indicate the presence of destressing zones. Their horizontal range is very limited and their destressing efficiency is very low. Seismic tomography does not reveal clearly the destressing zones as a result of previous mining of adjacent coal seams.
- In contrast to the analytical modeling results obtained before the commencement of mining operations, seismic tomography permits us to take into account the impact of the longwall face on the state of stress.
- Analytical modeling generally indicates bottom heading (IXa) as burst-prone, while seismic tomography points to the top heading (Xb west). Nevertheless, regarding the unfavorable location of the cut-through, the results obtained by the two methods appear to be reasonable.
- The observed seismicity developed in the course of mining operations appears to confirm the analytical modeling results relating to the occurrence of non-favorable conditions in the longwall panel. These conditions may potentially lead to degradation processes in the coal seam and adjacent rock layers and, consequently, trigger the occurrence of low-energy tremors.
- The results of both methods proved to be unreliable in the context of locating seismic foci within the longwall panel. The distribution of tremors in the analyzed energy intervals was rather random and did not coincide with

stress concentration zones determined by seismic and analytical methods.

With regard to complex conditions, seismic and analytical methods prove to be useful tools providing vital information for mining practice, particularly at the stage of engineering design and mining operations. A variety of modeling research techniques and methods yield complementary results. Their successive development, especially measurement apparatus and techniques, criteria for interpretation of results, accuracy and precision of mathematical models, will improve the reliability of the results obtained.

Compliance with ethical standards

Conflict of interest The authors declare that there is no conflict of interest.

Open Access This article is licensed under a Creative Commons Attribution 4.0 International License, which permits use, sharing, adaptation, distribution and reproduction in any medium or format, as long as you give appropriate credit to the original author(s) and the source, provide a link to the Creative Commons licence, and indicate if changes were made. The images or other third party material in this article are included in the article's Creative Commons licence, unless indicated otherwise in a credit line to the material. If material is not included in the article's Creative Commons licence and your intended use is not permitted by statutory regulation or exceeds the permitted use, you will need to obtain permission directly from the copyright holder. To view a copy of this licence, visit <http://creativecommons.org/licenses/by/4.0/>.

References

- (A-G) Agos-Gemes Sp. z o.o. (2009–2010) Badania geofizyczne dla oceny stanu naprężeń i zagrożenia tąpnięciami w rejonie projektowanej ściany nr 09a w pokładzie 501 w polu B1: I, II, III, IV seria (materiały niepublikowane) [Geophysical surveys for the assessment of stress and burst hazard in the area of the designed longwall no. 09a in deposit 501 in the field B1—I, II, III, IV series (unpublished materials)]
- Bańka P (2004) Determination of potential level of rockburst hazard based on the result of analytical predictions of stress distributions and the level of induced seismicity. *Acta Geodyn et Geomater* 11(1):19–26
- (BN-T) Biuro Naukowo-Techniczne Geotech II (2008) Ocena stanu naprężeń i zagrożenia tąpnięciami oraz wskazanie zasad profilaktyki tąpniowej w polu ściany nr 09a w pokładzie 501 pole B1 (materiały niepublikowane) [Stress and burst hazard assessment and indication of the principles of burst prevention in the longwall area 09a in deposit 501 area B1 (unpublished materials)]
- Cai W, Dou L, Cao A, Gong S, Li Z (2014) Application of seismic velocity tomography in underground coal mines: a case study of Yima mining area Henan, China. *J Appl Geophys* 109:140–149
- Cao A, Dou L, Cai W, Gong S, Liu S, Zhao Y (2016) Tomographic imaging of high seismic activities in underground island longwall face. *Arab J Geosci* 9:1–10
- Chlebowski D (2009) Wpływ wybranych parametrów geomechanicznych na kształtowanie się przemieszczeń i naprężeń pionowych w sąsiedztwie uskoku [The influence of selected geomechanical

- parameters on the formation of vertical displacements and stresses in the vicinity of the fault]. *Przegląd Górniczy*, nr 1–2:1–7
- Chlebowski D (2013) Analizy i modele modelowania eksploatacji skrzepowanej w aspekcie identyfikacji stref zagrożonych tąpnięciami [Analytical modeling of constrained exploitation in the aspect of identification of burst hazard areas], *Rozprawy-Monografie*, nr 290, Wydawnictwo AGH
- Czarny R, Pilecki Z, Nakata N, Pilecka E, Krawiec K, Harba P, Barnaś M (2019) 3D S-wave velocity imaging of a subsurface disturbed by mining using ambient seismic noise. *Eng Geol* 251:115–127
- Dou L, Chen T, Gong S, He H, Zhang S (2012) Rockburst hazard determination by using computed tomography technology in deep workplace. *Saf Sci* 50:736–740
- Dubiński J (1989) Sejsmiczna metoda wyprzedzającej oceny zagrożenia wstrząsami górnictwem w kopalniach węgla kamiennego [Seismic method of anticipating assessment of rockburst hazard in hard coal mines], *Prace naukowe Głównego Instytutu Górnictwa*
- Gil H (1991) *The theory of strata mechanics*, Wydawnictwo PWN
- Goszcz A, Dubiński J, Dworak J (1989) Praktyczne aspekty zastosowania tomografii sejsmicznej w górnictwie podziemnym [Practical aspects of the application of seismic tomography in underground mining]. *Wybrane zagadnienia lokalizacji ognisk wstrząsów górniczych i geotomografii sejsmicznej*, Główny Instytut Górnictwa, pp 86–120
- He H, Dou L, Li X, Qiao Q, Chen T, Gong S (2011) Active velocity tomography for assessing rock burst hazards in a kilometer deep mine. *Min Sci Technol* 21(5):673–676
- Hosseini N, Oraee K, Shahriar K, Goshtasbi K (2012) Passive seismic velocity tomography on longwall mining panel based on simultaneous iterative reconstructive technique (SIRT). *J Cent South Univ* 19:2297–2306
- Karfakis MG, Wu X (1995) Prediction of bump hazards associated with coal mining under competent roofs. In: *Rock Mechanics*, Daemen & Schultz (eds), AA Balkema Publishers
- Kłeczek Z (1994) *Geomechanika górnictwa* [Mining Geomechanics], Śląskie Wydawnictwo Techniczne
- Kłeczek Z, Małoszewski J, Parysiewicz S, Zorychta A (1987) Geomechaniczne kryteria zagrożenia tąpnięciami przy eksploatacji pokładów węgla kamiennego [Geomechanical criteria of rock burst hazard during exploitation of hard coal seams], Główny Instytut Górnictwa
- Kłeczek Z, Zorychta A (1990) Wpływ zaszłości eksploatacyjnych na stan naprężenia górotworu zagrożonego tąpnięciami [Influence of the exploitation remnants on the stress state of the rock mass at risk of rock burst], *Zeszyty Naukowe Politechniki Śląskiej, Górnictwo*, z. 185
- Kormendi A, Bodoky T, Hermann L, Dianiska L, Kalman T (1986) Seismic measurements for safety in mines. *Geophys Prospect* 34(7):1022–1037
- Krajewski C, Dresen L, Gelbke C, Ruter H (1989) Iterative tomographic methods to locate seismic low-velocity anomalies: a model study. *Geophys Prospect* 37:717–751
- Li X, Gong S, Dou L, Chai Y (2020) Detection of stress redistribution in a complex isolated coal pillar with active SVT technology. *Arab J Geosci* 13:1–12
- Lo T, Inderwieser PL (1994) *Fundamentals of seismic tomography*, Society of Exploration Geophysicists
- Luxbacher K, Westman E, Swanson P, Karfakis M (2008) Three-dimensional time-lapse velocity tomography of an underground longwall panel. *Int J Rock Mech Min Sci* 45(4):478–485
- Marcak H, Pilecki Z (2019) Assessment of the subsidence ratio based on seismic noise measurements in mining terrain. *Arch Min Sci* 64(1):197–212
- (Materials) *Materiały wewnętrzne kopalni* (2010) (materiały niepublikowane) [Own materials of the mine (unpublished materials)]
- Mutke G, Dubiński J, Lurka A (2015) New criteria to assess seismic and rock burst hazard in coal mines. *Arch Min Sci* 60(3):743–760
- Nolet G (1987) *Seismic Tomography*. D. Reidel Publishing Company, Dordrecht
- Pietuchow IM, Linkov MA (1979) The theory of post-failure deformations and the problem of stability in rock mechanics. *Int J Rock Mech Min Sci Geomech Abstr* 16(2):57–76
- Pilecki Z (1999) Dynamic analysis of mining tremor impact on excavation in coal mine, *Proc. FLAC Symp. on Numerical Modeling in Geomechanics*, Detournay & Hart (eds), 1–3 Sept. 1999, Minneapolis, USA, 397–400
- Ruban AD, Chernyakov AB, Zagorskii LS, Navikov AN (1993) Tomographic methods of wave-field reconstruction in problems of geomechanical monitoring. *J Min Sci* 29:228–234
- Saustowicz A (1968) *Zarys mechaniki górotworu* [Fundamentals of strata mechanics], Wydawnictwo Śląsk
- Szreder Z, Pilecki Z, Kłosiński J (2008) Effectiveness of recognition of exploitation edge influence with the help of profiling of attenuation and velocity of seismic wave, *Gospodarka Surowcami Mineralnymi*, t. 24, 2/3, 215–226
- Wang S, Lam K, Au S, Tang C, Zhu W, Yang T (2006) Analytical and numerical study on the pillar rockbursts mechanism. *Rock Mech Rock Eng* 39(5):445–467
- Wang G, Gong S, Li Z, Dou L, Cai W, Mao Y (2016) Evolution of stress concentration and energy release before rock bursts: two case studies from Xingan Coal mine Hegang, China. *Rock Mech Rock Eng* 49:3393–3401
- Yang J, Chen W, Tan X, Yang D (2018) Analytical estimation of stress distribution in interbedded layers and its implication to rockburst in strong layer. *Tunn Undergr Space Technol* 81:289–295
- Zhao C, Hebblewhite BK, Galvin JM (2000) Analytical solutions for mining induced horizontal stress in floors of coal mining panels. *Comput Methods Appl Mech Eng* 184:125–142
- Zorychta A (2003) *Geomechaniczne modele górotworu tąpającego* [Geomechanical models of bursting rock mass], Wydawnictwo Instytutu Gospodarki Surowcami Mineralnymi i Energią PAN
- Zorychta A, Burtan Z (2008) Uwarunkowania i kierunki rozwoju technologii podziemnej eksploatacji złóż w polskim górnictwie węgla kamiennego [Conditions and future directions for technological developments in the coal mining sector], *Gospodarka Surowcami Mineralnymi* t. 24 z. 1/2, 53–70
- Zorychta A, Chlebowski D (1998) Wpływ wybranych parametrów naturalnych i technologicznych na zagrożenie tąpnięciami w warunkach oddziaływania zaszłości eksploatacyjnych [Influence of selected natural and technological parameters on the rock burst hazard in the conditions of exploitation remnants]. *Prace Naukowe Głównego Instytutu Górnictwa*, nr 26:149–164
- Zorychta A, Burtan Z, Chlebowski D (1999) Metoda określania stanu zagrożenia tąpnięciami w sąsiedztwie dyslokacji tektonicznych [The method for determining the state of burst hazard in the vicinity of tectonic dislocations]. *Czasopismo Naukowo-Techniczne Górnictwa Rud, Cuprum*, nr 10:13–26